Physics-Informed Neural Networks Applied to Catastrophic Creeping Landslides

Ahmad Moeineddin[1*], Carolina Seguí[2], Stephan Dueber[1] and Raúl Fuentes[1]

[1*]Chair of Geotechnical Engineering and Institute of Geomechanics and Underground Technology, RWTH-Aachen, Mies-van-der-Rohe-Str. 1, Aachen, D-52074, Germany.
[2]Department of Crystallography, Mineralogy and Mineral Deposits, Faculty of Geology, University of Barcelona, Spain.

*Corresponding author(s). E-mail(s): Ahmad.moeineddin@rwth-aachen.de;
Contributing authors: carolina.segui@ub.edu; dueber@gut.rwth-aachen.de; raul.fuentes@gut.rwth-aachen.de;

Abstract

In this study, a new paradigm compared to traditional numerical approaches to solve the partial differential equation (PDE) that governs the thermo-poro-mechanical behavior of the shear band of deep-seated landslides, is presented. In particular, we show projections of the temperature inside the shear band as a proxy to estimate catastrophic failure of deep-seated landslides. A deep neural network is trained to find the temperature, by using a loss function defined by the underlying PDE and field data of three landslides. To validate the network, we have applied this network to the following cases: Vaiont, Shuping and Mud Creek landslides. The results show that, by creating and training the network with synthetic data, the behavior of the landslide can be reproduced and can forecast the basal temperature of the three case studies. Hence, providing a real-time estimation of the stability of the landslide, compared to other solutions whose stability study has to be calculated individually for each case scenario.

Moreover, this study offers a novel procedure to design a neural network architecture, considering stability, accuracy, and over-fitting. This approach could be useful also to other applications beyond landslides.

Keywords: PINNs, Numerical modeling, Landslides, Shear band, Temperature

1 Introduction

The behaviour of catastrophic rapid landslides has been studied by many researchers in the past. The aim of these studies has been to understand the mechanisms of failure and obtain an approximate time of failure (i.e., when the landslide turns unstable, transitioning from secondary creep to a tertiary creep phase). The first approach to predict the time of failure used the inverse velocity of the sliding mass of the landslide. When the landslide reaches the last acceleration, the inverse of velocity is extrapolated until zero, which is the predicted time at which the landslide will collapse Voight (1988); Saito (1965, 1969). However, this kind of prediction does not take into consideration the mechanisms of failure, and gives a very short period of time (minutes) of early-warning before the landslide collapses catastrophically. Other studies have focused on one of the weakest part of the landslide, which is the shear band Kilburn and Petley (2003). Inside the shear band of the landslide, all the thermo-mechanical phenomena take place Vardoulakis (2002b); Veveakis et al (2010, 2007); Goren and Aharonov (2009). Therefore, recent studies have focused on how the external loading (e.g., groundwater variations) affects the material behavior of the shear band (e.g., friction coefficient) Alonso and Pinyol (2010); Alonso et al (2016).

Moreover, most shear bands of deep-seated landslides are formed by clay or clayey materials, which can exhibit a thermal softening behavior Vardoulakis

(2002a,b); Hueckel and Baldi (1990). Thus, when the landslide accelerates the material of the shear band enters a positive thermal feedback loop Vardoulakis (2002b); Veveakis et al (2007) that can trigger mechanical dissipation by increasing the temperature and reducing the friction coefficient of the material Anderson (1980); Vardoulakis (2002b); Voight and Faust (1982); Lachenbruch (1980); Rice (2006). This process of positive thermal feedback loop can continue until the shearing resistance of the material decreases uncontrollably because of a thermal runaway instability occursGruntfest (1963), which, after the bifurcation point, can happen without any variation of loading conditions (external factors).

New models consider the above phenomena. First, Vardoulakis (2002b) presented a mathematical model assuming that the coupling mechanisms that affect the clay material of the landslide's gouge are the counterbalance between the thermal softening and the rate hardening. Veveakis et al (2007) applied this mathematical model to the Vaiont landslide, assuming only the maximum loading condition (highest groundwater level), not changing in time. The authors considered the increase of temperature inside the shear band during the last two years of the creeping phase of the landslide until the collapse. Their results showed that the landslide collapsed because the material of the shear band reached the positive thermal feedback loop to a point that, despite the effort of reducing the external loading (groundwater level), the material reached its critical value of basal temperature and became unconditionally unstable.

Later, Segui et al (2020) applied the same mathematical model for a time-dependent external load to two case studies: the Vaiont and the Shuping landslides. Both of these landslides are activated due to the construction of a dam and their behavior depends on the evolution of the water level of the dam. The results of the model applied to those case studies, show the critical

point of stability for the Vaiont landslide and the critical value of temperature. Conversely, Shuping is currently active, and the model has been used to quantify the effect of external loading and obtain the optimal water level of the dam for the landslide to stay in the secondary creeping phase (i.e., stable).

Afterwards, the theoretical assumption of the role of temperature in the material behavior of a deep-seated landslide has been tested and validated by Seguí et al (2021). The authors installed a thermometer inside the shear band of an active deep-seated landslide, El Forn landslide in Canillo (Andorra). The field data shows that the clayey shear band is thermal sensitive, and increases its temperature when the water pressure increases, and then the landslide accelerates. For this case, the clayey material, which consists of shales of the Silurian period, is very sensitive to changes in external loading (water pressure) and reduces its shearing resistance and allows the landslide to accelerate. For this case, the authors had also applied the mathematical model showing how stable the active landslide is, and allowing to understand what causes the instability and acceleration of the landslide.

In a more recent paper, Seguí and Veveakis (2022) presented the mathematical model applied to four case studies: the Vaiont, the Shuping, the El Forn, and the Mud Creek landslides. Where all of them have been mapped in the stability curve (steady-state/bifurcation curve), showing that the model, which is simplified to basal temperature - Gruntfest number (i.e., external loading) can be applied to different deep-seated landslides, regardless of the nature of their instability and/or the data available (properties of the shear band material and field data).

The latter model by Vardoulakis (2002b); Veveakis et al (2007); Segui et al (2020) proposed a partial differential equation (PDE) that is able to capture the interplay between the external loading (e.g., groundwater variations)

and the basal (shear band material) temperature through the heat diffusion equation in dimensionless form. This equation depends on two parameters: the basal temperature and the Gruntfest numbera bifurcation parameter called the Gruntfest number Gruntfest (1963), which is plotted in a steady-state curve which is also called bifurcation curve calculated through the heat diffusion equation in dimensionless form as steady-state and applying the pseudo-arc-length continuation method. This PDE allows to map the behavior of the landslide in time on the bifurcation curve, thus forecasting when the landslide will turn unstable (i.e., transitioning from secondary to tertiary phase) and collapse catastrophically. As mentioned above, the constitutive model considers that the shear band material behaves as rate hardening and thermal softening:

$$\frac{\partial \theta^*}{\partial t^*} = \frac{\partial^2 \theta^*}{\partial {z^*}^2} + Gr\, e^{\theta^*} \tag{1}$$

where θ is the temperature, t is time, z is the thickness of the shear band, and Gr is the Gruntfest number, which is a ratio of the mechanical work that is transformed to heat over the materials heat diffusion capacity. Gr contains information about the basal mean shear stress (including the effects of groundwater evolving in time), thermal conductivity, shear band thickness and reference shear strain rates (see (Segui et al, 2020) and (Veveakis et al, 2007) for more information about the mathematical model). It is therefore a convenient way to encapsulate multiple data which benefits the work in this paper, as will be shown later.

This equation (1) is complex to solve and current solutions involve using the pseudo arc-length continuation method with spectral elements using Fourier transforms, instead of finite elements or other more traditional approaches (Veveakis et al (2010); Chan and Keller (1982); Segui et al (2020).

If an equally accurate model was available, that could make predictions in real-time and update much quicker, this would offer significant advantages to make timely predictions to compare with observations. Thus, we propose an alternative solution using artificial neural networks that have shown their potential in a range of computational tasks. Their universal approximation features offer a novel ability to solve differential equations DeVore (1998); Tariyal et al (2016); Hangelbroek and Ron (2010). Recent applications of this data-driven paradigm include earthquake detection Yoon et al (2015); Berg and Nyström (2018), fluid mechanics and turbulence modeling Brunton et al (2020); Brenner et al (2019), dynamical systems Rafiei and Adeli (2017), and constitutive modeling Butler et al (2018); Brunton and Kutz (2019).

It requires the cooperation of two essential factors. The first one is a parameterized function that is both easy to train and evaluate, and robust enough to approximate the solution of a complicated PDE. Modern deep neural network models, LeCun et al (2015), provide these functions, which are made up of a number of linear transformations and component-wise non-linearities. Because of recent developments in paralleled hardware and automatic differentiation Bergstra et al (2010); Baydin et al (2018); Ermoliev and Wets (1988), deep neural network models with numerous parameters can be trained and assessed rapidly. The other essential component is a loss objective or function. A loss function, when reduced, promotes that the parameterized function is a satisfactory approximation solution of the PDE.

This approach is now known as Physics-Informed Neural Networks (PINNs). It has been applied to numerous forms of PDEs representing different phenomena in physics and engineering (see Raissi et al (2019)). Critical to this approach is the use of automatic differentiation (AD) has made a significant contribution to enable this approach, as shown by Griewank et al (1989).

It allows obtaining derivatives of the output variable with regard to the input parameters. Other methods of calculating the derivatives suffer from rounding-off errors and therefore, lead to inaccuracies Baydin et al (2018). This drawback of other approaches is avoided in PINNs by using modern graph-based implementations such as TensorFlow Abadi et al (2016) or PyTorch Paszke et al (2017). Using this automatic differentiation, exact expressions with floating values are applied, and no approximation error is found. In PINNs, the solution of the PDE is predicted without the need of an additional model, by including the PDE in the neural network loss function. Hence, during learning, the Neural Network (NN) learns to minimise the residual of the PDE using the learnt input parameters. Boundary and initial conditions are also included in the loss function in different ways to complete the boundary value problem.

The advantage is that a PINN model may be used as a surrogate model for a range of input parameters, allowing for real-time simulation. A PINN also has other several advantages over the finite element method and other surrogate models: it does not require a mesh-based spatial discretization or laborious mesh generation; the derivatives of the solutions are available after training; it satisfies the strong form of the differential equations at all training points with known accuracy; and it allows data and mathematical models to be integrated within the same framework Pang and Karniadakis (2020).

As mentioned previously, PINNs have been applied to a variety of problems, including fluid mechanics Cai et al (2022); Wu et al (2018); Jin et al (2021), solid mechanics Haghighat et al (2021); Rao et al (2021); Guo and Haghighat (2020), heat transfer Niaki et al (2021); Cai et al (2021b), and soil mechanics Bandai and Ghezzehei (2021); Amini et al (2022), including multiple ground-based problems Amini et al (2022). However, to our knowledge, never to landslides in general, and certainly more specifically to catastrophic

deep-seated landslides where the formulation of Eq. 1 allows us to apply this approach.

Hence, this paper starts with a short introduction to three different case studies we have used to validate our approach, then we introduce the basics of PINNs using the general problem we focus on, followed by a presentation and discussion of the results in the context of three known case studies. In the end, we present the conclusions of this paper.

2 Case studies

Three deep-seated landslides are used in this study: Vaiont, Shuping and Mud Creek, which are briefly explained below. Detailed descriptions of the case studies can be found in Seguí (2020); Segui et al (2020); Seguí and Veveakis (2022); Handwerger et al (2019); Alonso et al (2016). The description below is limited to the different trigger mechanisms, landslide volumes and failure stages, in order to highlight the varied conditions that can be covered. Interestingly for this paper, Figure 1 shows the Gruntfest number calculated for each case study as a function of time Seguí (2020); Seguí and Veveakis (2022). As will be shown later, the different order of magnitude, comparing Shuping (still in secondary creep) with Mud Creek and Vaiont (already failed) can be a problem that can be overcome to obtain a good generalisation. Table 1 presents a summary of the characteristics of each case study.

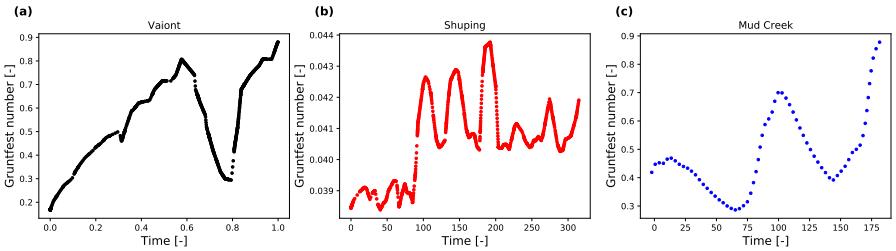

Fig. 1 Gruntfest number in time with time-dependent external loadings history for different case studies Seguí (2020); Seguí and Veveakis (2022) , (a) The Vaiont landslide (Italy) that collapsed in 1963, (b) The Shuping landslide in the Three Gorges Dam (China) that remains active, (c) The Mud Creek landslide in California (USA) that collapsed in 2017.

2.1 Vaiont, Italy

The Vaiont landslide was an ancient landslide reactivated by the filling process of a dam constructed nearby Sem (1992). While the dam was working, the field data was showing that when the water level of the dam increased, the landslide accelerated. Thus, the engineers of the dam were controlling the accelerations of the landslide by reducing the water level of the dam MULLER (1964); Müller (1968). That happened because the material of the sliding mass was mainly calcarenite and limestone with high permeability Ferri et al (2011). On October 9th, 1963, the landslide catastrophically failed mobilising approximately 270 million m^3 of material over a depth of 150 m MULLER (1964); Müller (1968). The material reached velocities in excess of 20 m/s resulting on a tsunami that over-topped the dam causing significant destruction downstream and 2000 casualties.

2.2 Shuping, China

The Shuping landslide was reactivated by the construction of the Three Gorges Dam in China. Additionally to the reservoir water level, the area is also subject to long periods of rainfall, which has been highlighted as another possible

factor for triggering Segui et al (2020); Huang et al (2016). The lithology of the area is mainly sandy mudstone and muddy sandstone Wang et al (2017). The thickness of the landslide is between 30 and 70 m and has a calculated volume of 27 million m^3. Conversely to Vaiont, this landslide accelerates during reservoir lowering and slows down during filling Segui et al (2020); Huang et al (2016). The difference possibly resides in the different permeability of the sliding mass above the shear band Segui et al (2020).

From the point of view of this paper, it is critical to highlight that Shuping has not catastrophically failed as indicated by the low Gruntfest numbers shown in figure 1. The fact that it shows also a different behaviour to Vaiont reinforces the ability to capture different phenomena.

2.3 Mud Creek, USA

Mud Creek was a landslide, that like Vaiont, catastrophically collapsed on May 20th of 2017 in California (USA) Handwerger et al (2019). The thickness of the landslide material was 20 m and approximately 60 million m^3 of material collapsed, failing into the sea and destroying a coastal road Handwerger et al (2019). The triggering mechanism is not clear, but it is speculated that a combination of earthquakes and transition from extreme droughts to extreme rainfall were the main causes of the failure Handwerger et al (2019).

Table 1 Case Study Summary

Landslide	Volume($1E^6 m^3$)	Thickness(m)	Potential cause
Vaiont	270	150	Reservoir water level rise leading to reactivation
Shuping	27	30-70	Three Gorges Dam reservoir filling
Mud creek	60	20	Reactivation due to precipitation, earthquakes

3 PINNS basics and problem application

All neural networks need consideration of three main general aspects: network architecture, loss functions and training. They are explained below in the context of our application. A more detailed theoretical and methodological explanation for each can be found, for example, in Haghighat and Juanes (2021); Raissi et al (2019).

3.1 Network architecture

The typical architecture of PINNs uses Feed-Forward Neural Networks Schmidhuber (2015) (FFNNs), as presented in figure 2. It has Z as an input tensor and u as an output tensor, and it includes network trainable parameters, such as weights, W, and biases, b. In the application to Eq. 1, the input Z consists of three variables: z, t and Gr. The output tensor u is the temperature θ.

When deciding an architecture of NN, a decision needs to be made on the number of layers and number of neurons in each layer. The number of hidden layers is an arbitrary, but very important aspect. It can be chosen based on the number of collocation points and the number of input and output parameters, but its selection remains largely a trial-and-error process. In some implementations, this number is considered a hyper-parameter, and therefore, can be fine-tuned during training. Equally, it can also be included as an additional variable so that its value is part of the learning process. However, consensus is not clear as to what approach is more adequate and therefore, lacking an established and rigorous way to do it, we propose later a systematic framework to choose it that we consider a novel contribution of our paper.

In this type of fully connected neural network, neurons in a layer have no connection to each other Bishop and Nasrabadi (2006). This FFNNs can be shown mathematically as shown in Eq. 2:

$$u^k = \sigma^k(W^k\ Z^{k-1} + b^k), \qquad k = 1, ..., K \tag{2}$$

where $Z^0 = X$ is the input layer and u^k is the output layer. The values of the output layer are approximated as a function of the weights, W, and biases, b. Each connection between a neuron in layer *k-1* and another neuron in layer k is assigned a weight W and a bias term b. Taking the weighted sum of its inputs, $Z^k - 1$, as well as a bias term, it delivers the output through an activation function σ that accommodates non-linearity Sibi et al (2013).

3.2 Loss function

In traditional FFNNs, the loss function can be calculated by minimizing the square of difference of the predicted and given outputs Schmidhuber (2015), or the so-called Mean Square Error *MSE* (equation 3).

$$MSE = \sum_{i=1}^{n} (Y_i - \overline{Y}_i)^2 \tag{3}$$

where n is the total number of collocation points, and Y and $\overline{Y}$ are the ground truth values and the predicted values, respectively. As previously mentioned, in PINNs, the physics are included by adding the PDE to the loss function. Therefore, the total Loss, $\mathcal{L}$, becomes:

$$\mathcal{L} = \mathcal{L}_{data} + \mathcal{L}_{PDE} \tag{4}$$

where $\mathcal{L}_{data}$ is the loss function calculated from data points as in traditional FFNNs, and $\mathcal{L}_{PDE}$ is the loss function from considering the physics using the PDE and the initial value. Generally, this will also involve adding boundary condition losses, but these do not apply to the problem we are solving here. Hence, the PDE loss function is:

$$\mathcal{L}_{PDE} = \mathcal{L}_{\theta} + \mathcal{L}_{\theta_0} \tag{5}$$

We can then write equation 1 into the mean squared error loss function as:

$$\mathcal{L}_{\theta} = \frac{1}{n}\sum_{i=1}^{n}\left(\frac{\partial\theta^*}{\partial t^*}|_{z_i} - \frac{\partial^2\theta^*}{\partial {z^*}^2}|_{z_i} - Gr\ e^{\theta^*}|_{z_i}\right)^2 \tag{6}$$

The losses related to the initial condition are calculated as:

$$\mathcal{L}_{\theta_0} = \frac{1}{n}\sum_{i=1}^{n}\left(\theta|_{t=0} - \theta_0(z)\right)^2 \tag{7}$$

Finally, the network is trained by minimizing the losses for a different set of hyper-parameters, θ, at the collocation points, X:

$$\theta^* = \arg\min_{\theta} \mathcal{L}_N(X;\ \theta) \tag{8}$$

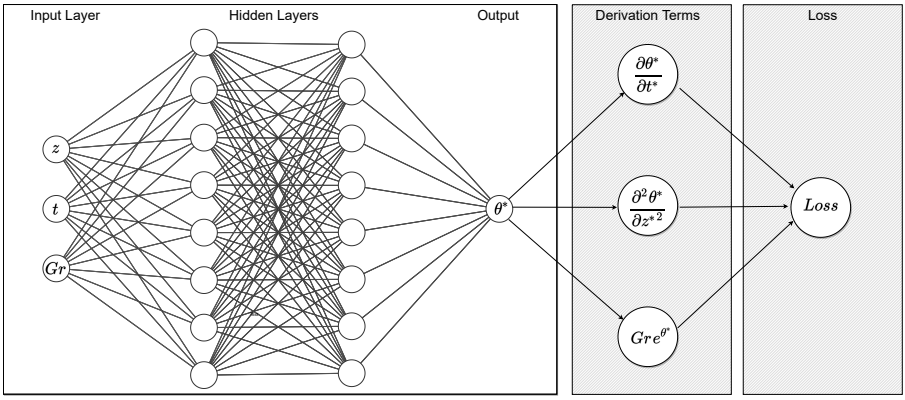

Fig. 2 A schematic of single neural network architecture with space, time, and Gruntfest number as input features (z; t; Gr). And the temperature, θ, as output with optimization of the total loss function, consisted of loss terms for the governing equation.

3.3 Training

Training is the third critical part of the PINNs. One of the critical parameters in the process of training PINNs is the activation function, which should be chosen considering the partial differential equation and the physical output quantities. After considering different activation functions, and comparing the final value of the loss function, we observed that *tanh* gave the best results with the lowest loss function. We also used (*tanh*, *sigmoid*, *swish*, and *softplus*), although this comparison is not included in the paper. The *tanh* activation function can be defined as:

$$\tanh(n) = \frac{\exp^{n} - \exp^{-n}}{\exp^{n} + \exp^{-n}} \tag{9}$$

We used the available algorithms in Keras Chollet et al (2015) and Adam's optimization scheme Kingma and Ba (2014) within the SciANN Haghighat and Juanes (2021) framework for training. Due to the lack of an systematic approach, we defined the learning rate using trial and error. The learning rate is a hyper-parameter worth tuning because of the use of the stochastic gradient descent algorithm. We reached the conclusion that 0.001 is a suitable value for the learning rate, since the optimizer can reach the minimum value slowly, whilst avoiding getting stuck in local minima. It also needs to be considered that, adaptive learning is included in SciANN, and the optimizer (in our case, Adam) reduces the value of the learning rate in case it is necessary. Hence, this value was not critical for this implementation.

Different hyper-parameters and architectures are investigated in this study. The hyper-parameters in the algorithm, which had a noticeable influence during the training of this problem, are *batch-size*, *activation function*, and *number*

of epochs. Batch size is the number of collocation points from a data set, used to determine one gradient descend update Ruder (2016). The batch size also influences the computational cost. This means that, for a larger batch size, the training becomes faster because less iterations are needed for one epoch to round the training on a data set. The minimum batch size is 1, which corresponds to a full stochastic gradient descent optimization. In this work, several different batch sizes were considered to find the best and optimal value, which in this case was 64.

The second important hyper-parameter is the number of epochs. At each epoch, before a new round of training (epoch) starts, the data set can be shuffled leading to an updated parameter. This occurs when the batch-gradients are calculated on a new batch and therefore, it is affected by the number of batches. In PINNs, a value of 5000 epochs was used in several studies Raissi et al (2019); Niaki et al (2021) and we have used it here after trial and error, using as criteria a predefined low-value of the loss function as recommended by Raissi et al (2019). In many cases, the total loss converges to a constant value after 3000 epochs. Shuffling of collocation points was also used during the training.

Since the aim of this study is to minimize the loss function, and since the optimizer is non-convex, the training needs to be tested from different starting points and, at the same time, with different directions. In this way, weights and biases are evaluated by minimizing the loss function, and patience is a limit that monitors the optimizer intended to stop the training.

Over-fitting during the training Hawkins (2004) is always a concern, especially for forecasting unseen cases. Since the number of collocation points in this study is small, the over-fitting is examined by splitting the collocation points into three sets: train, test, and validation. Since validation data are

available during training, the accuracy and loss function can be plotted in Keras Chollet et al (2015) for examination. This offers a great advantage to control over-fitting. If during training, the loss function increases, or the model starts to lose test accuracy, then the model is over-fitted.

There are several methods to train the PINNs. In this research, calculated data from Segui et al (2020); Seguí and Veveakis (2022) is used for training, which is presented in the next section.

4 Synthetic data and network architecture

4.1 Synthetic data

The purpose of PINNs is to generate a model with good generalization properties. Initially, one typically trains the model using only the PDE, without any data. In our case, the results of doing this were not satisfactory, hence this approach was abandoned. This is due to the complexity contained by the Gr, which is not captured when considering only the PDE. Hence, training with data was necessary.

Figure 3 shows the results where the training and testing has been performed individually for each case. As expected, the results are very close to the initial data when training in the same case. Note that the used architecture for this case is 4 hidden layers and 10 neurons for each one. As Fig. 3 shows, this is not the optimal architecture, however the temperature calculated reproduces the behavior of the ground truth with minor discrepancy.

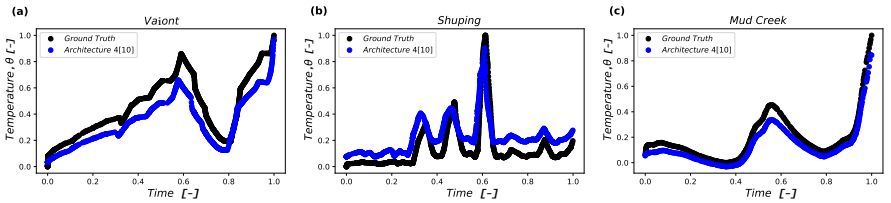

Fig. 3 Normalized Temperature evolving in time for the three case studies applying the architecture of 4[10]. Here, the training and the testing has been performed individually for each case study. Note that the Ground Truth data is from Segui et al (2020); Seguí and Veveakis (2022): (a) Ground truth and architecture data of the Vaiont landslide, (b) Ground truth and architecture data of the Shuping landslide, (c) Ground truth and architecture data of the Mud Creek landslide.

By using an optimal architecture with 3 layers and 20 neurons each, the results reproduce the ground truth with more accuracy as shown in Figure 4. However, one must understand that this is using training data selected randomly along the whole time domain (i.e., there is future prediction ability, but only interpolation) and within the same case study.

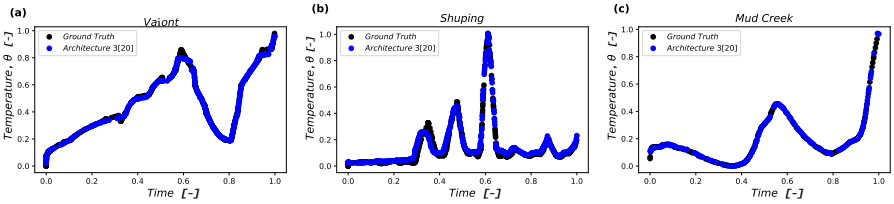

Fig. 4 Normalized Temperature in time for the three case studies with architectures of 3[20]. The training and the testing has been performed individually. Note that the Ground Truth data is from Segui et al (2020); Seguí and Veveakis (2022): (a) Ground truth and architecture data of the Vaiont landslide, (b) Ground truth and architecture data of the Shuping landslide, (c) Ground truth and architecture data of the Mud Creek landslide.

However, this approach hardly helps to generalize the behavior of all (unseen) case studies. As shown in Figure 5, we have trained the model with two of the cases and tested the model on the third one. We repeat this for all

three combinations (Fig. 5). As can be seen, the results are not as satisfactory. Critically, the model is not capable of forecasting the Shuping behavior. This means that generalize by training the model with just one landslide does not represent the behavior of the rest of case studies.

Therefore, the next option is to resort more data or create synthetic data. This approach has been followed by several authors Bandai and Ghezzehei (2021); Cai et al (2021a); Jagtap et al (2022). Hence, this method has been implemented in our study to define the best hyper-parameters and the optimal network architecture. The adequacy of this approach to represent real case studies is presented in the next section.

The synthetic data was generated by using the observations from Segui et al (2020) and Veveakis et al (2007). Those studies show that the Gruntfest number follows a sinusoidal wavy, increasing, pattern. This sinusoidal pattern is related to seasonal groundwater variation which leads to an increase in the temperature of the shear band and an acceleration of the sliding mass Cecinato et al (2008); Seguí et al (2021). It can be written as:

$$Gr = 0.8t + exp(t)(0.07sin(c * t)) \quad 0 < t < 1 \tag{10}$$

where Gr is the Gruntfest number, and t is the time. The equation is defined so that the maximum value of Gr is 0.88 as the critical value stated by Segui et al (2020), meaning that once the system reaches and overcomes this value, the system becomes unconditionally stable and the landslide enters the point of no return (i.e., tertiary creep, catastrophic collapse) Segui et al (2020). c covers the number of cycles or seasonal changes that the landslide experiences. Hence, by using an appropriate number of cycles and forcing it to fail by reaching a Gr equal or higher than 0.88, we can control that all possible behaviours are generally covered in the synthetic data. A value of c equal to

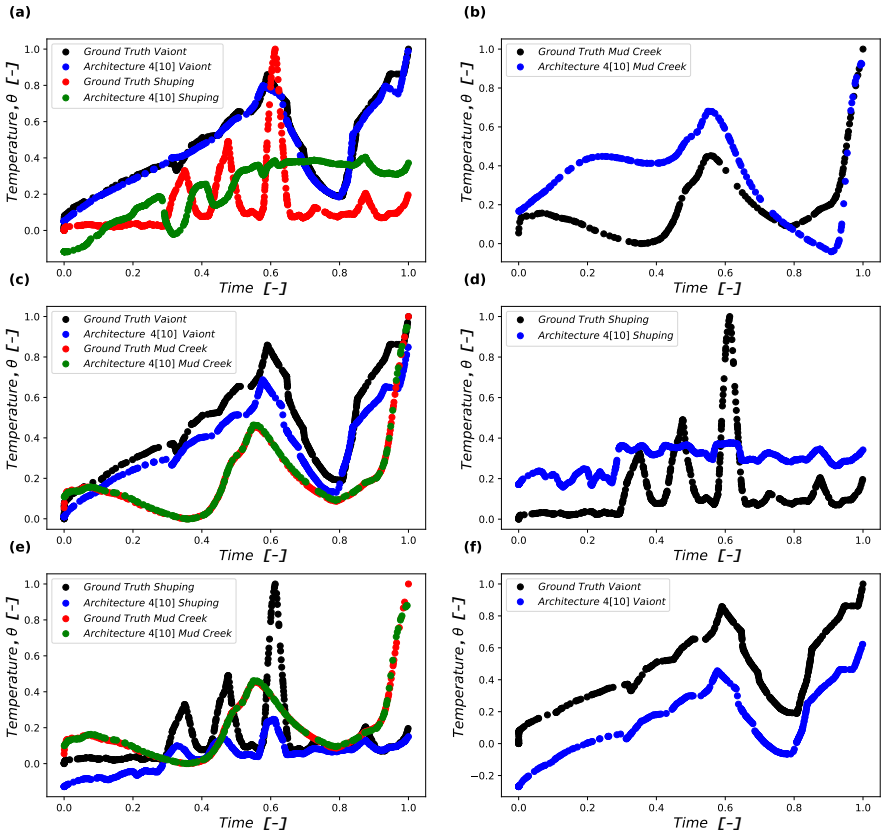

Fig. 5 Normalized Temperature in time for the three case studies by training two different cases and testing on the other one. Note that the Ground Truth data is from Segui et al (2020); Seguí and Veveakis (2022). (a) Training the model with the Vaiont and Shuping landslides, (b) Testing of the Mud Creek landslide by the training of Fig. 5a, (c) Training the model with the Vaiont and Mud Creek landslides, (d) Testing of the Shuping landslide by the training of Fig. 5c, (e) Training the model with the Shuping and Mud Creek landslides, (f) Testing of the Vaiont landslide by the training of Fig. 5e.

32 is used, which corresponds to five seasonal changes, taken as the behavior of the Shuping landslide, which is the case study with more years of data. The temperature is calculated using the method presented by Vardoulakis (2002b); Veveakis et al (2007); Segui et al (2020); Seguí et al (2021); Seguí and Veveakis (2022). The generated synthetic data is shown in Figure 9a.

A critical aspect of using PINNs is the normalisation of the data. In particular, in those cases where the variables show large differences in scale. For

example, the Gruntfest number in Shuping only varies between 0.038 and 0.044, whereas in Vaiont it reached the critical value of 0.88. Equally, the time is also at a different scale. Hence, we normalized all of the input and output variables between 0 and 1. Without this normalisation, none of the architectures and attempts were successful. In any event, this is generally a good practice Haghighat and Juanes (2021); Raissi et al (2019).

4.2 Network Architecture sensitivity analysis

In this section we present an approach to selecting the network architecture using a sensitivity analysis where we considered the number of neurons and number of hidden layers. We performed all of our training on the generated synthetic data, which contains 1510 collocation points. We always kept 10 percent of the data for testing after each training, and determine the convergence of the network in terms of over-fitting. We used the network hyper-parameters and activation function shown in section 3.3.

For the study of the optimal network architecture, the criteria we used from the sensitivity analysis was three-fold: minimising the loss function, reducing the standard deviation (stability) of network prediction for the unseen cases (which is due to the random process associated to different initial values of weights and biases for each network); and avoiding over-fitting.

Figure 6 shows the standard deviation, based on 5 realisations, in the y-axis and the error in the x-axis. The error is calculated as the mean absolute difference of the forecast values to the ground truth. It only shows combinations of layers and neurons (layers[neurons]), where over-fitting was not observed. The number of neurons was kept equal for all hidden layers, which is common for different implementations of PINNs Haghighat et al (2021); Raissi et al (2019). The plotted values in Figure 6 show the results for the three case studies.

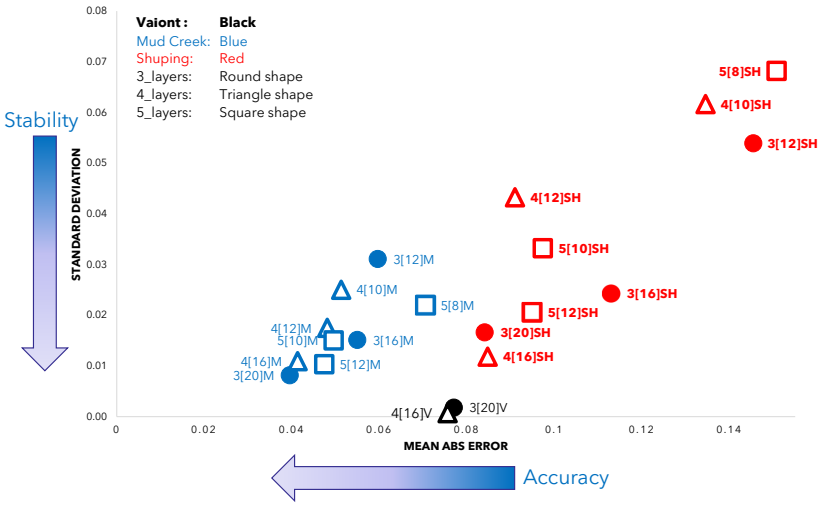

Fig. 6 Comparison of mean absolute error and standard deviation of the different network architectures by training the Synthetic Data and forecasting the three case studies. (Black) the Vaiont landslide results, (Red) the Shuping landslide results, (Blue) the Mud Creek landslide results. (Round) 3 hidden layers network, (Triangle) 4 hidden layers, (Square) 5 hidden layers.

Based on the results of the sensitivity analysis, the Vaiont case showed the highest stability of the network (i.e., each time the network is trained, the results are the same) among all cases. However, the accuracy of Vaiont almost remained constant throughout the different architectures. The case of Shuping is the most sensitive case to the architecture, and the standard deviation of different network architectures changed significantly. The case of Mud Creek showed the best accuracy of all cases. In general, the more neurons, the more accurate and network's stable the results are. The upper bound of neurons is provided by the over-fitting consideration.

After examining all the cases, we concluded that the best two architectures are: 1) using 3 hidden layers and 20 neurons per layer, and 2) 4 hidden layers with 16 neurons each. We repeated the training with these architectures

to calculate the value of the total loss function and validate our conclusion. Both networks showed a good convergence in terms of loss function, which is demonstrated in Figure 7 and also confirms that the PDE is satisfied.

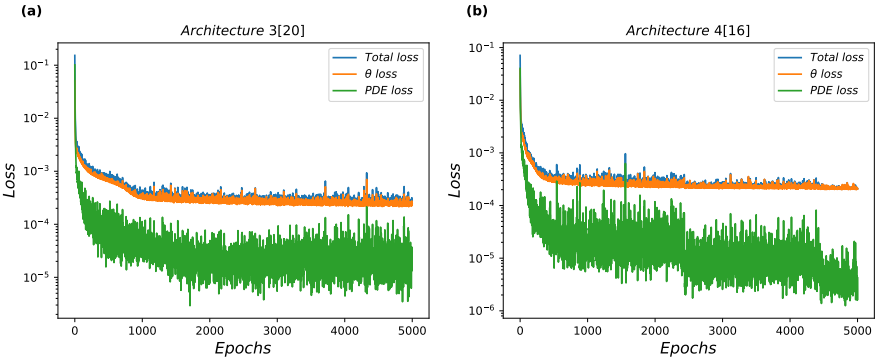

Fig. 7 Evolution of the different loss functions in the training of the network for synthetic data. The graphs also include the total loss, the loss from Temperature (θ), and the loss from the governing equation (Eq. 5). (a) Joint network architecture applying 3 layers and 20 neurons. (b) Joint network architecture applying 4 layers and 16 neurons.

To further examine the robustness of these two network architectures (Fig. 7), we calculated the 95% confidence range of each network. As presented in Figure 8, the repeated training on synthetic data shows a satisfactory performance, in terms of calculated loss function. The network stability training is considered satisfactory and, based on this training, we calculated the basal temperature of the three landslides.

5 Results and discussion

Figure 9 shows the results of the calculated temperature using only the synthetic data as training inputs, and the network architectures chosen in the previous section. These results expand on the parametric studies and are validated by fitting of the ground truth data from Segui et al (2020); Seguí et al (2021); Seguí and Veveakis (2022) with low absolute mean error as shown in Fig. 6. Moreover, we have validated the network in terms of trends and times

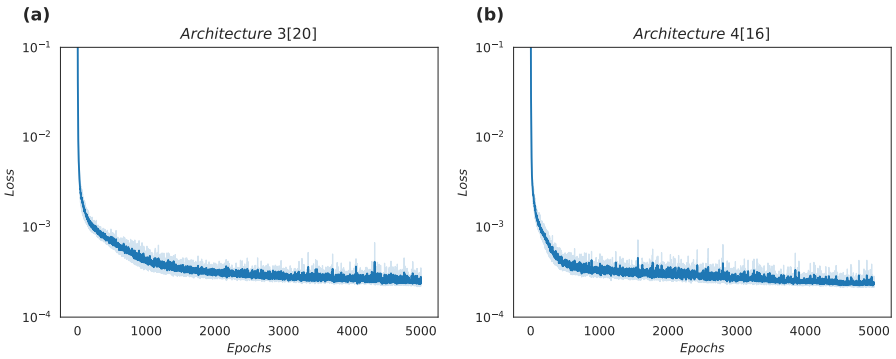

Fig. 8 Evolution of the 95% total loss confidence band of training the synthetic data for a) network architecture 3[20] and b) network architecture 4[16].

at which changes occur. By training the proposed synthetic data, we are able to forecast the point of instability (i.e., when the landslide reaches the point of no return and enters the tertiary creep) of the landslide in both, Vaiont and Mud Creek cases. At the same time, since the created synthetic data considers multiple seasonal changes, it could closely represent the real behavior of the Shuping landslide although they underestimate the temperature for the larger peak. The results of the network architecture with 3 layers and 20 neurons were slightly closer to the ground truth data. Since the suggested synthetic data can be regenerated for more seasonal changes, it is expected that by re-training the model, the core temperature of the shear band in other cases of deep-seated landslides could be also achievable. This is extremely important for practical purposes, if such a model is going to be used. For example, the model does not seem to reproduce the exact maximum temperature for all three cases. However, the calculated temperature by the network reproduces the changes of the behavior in time.

6 Conclusions

In this study, we present a physics-informed neural networks framework for modeling deep-seated landslides. The proposed PINN is a feed-forward neural

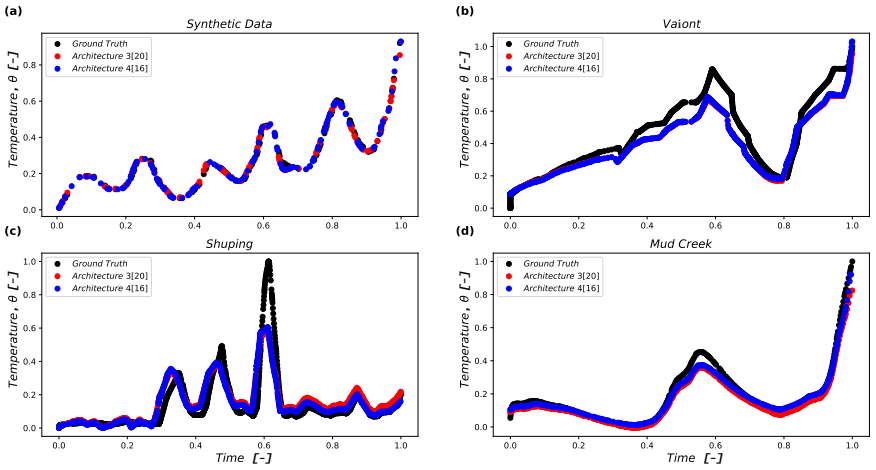

Fig. 9 Normalized Temperature in time calculated by the network for the three case studies. This normalized temperature has been calculated by training the synthetic data for two different network architectures 3[20] and 4[16]. Note that the Ground Truth data is from Segui et al (2020); Seguí and Veveakis (2022). (a) Fit of the ground truth (generated data) and calculated by the network Synthetic Data, (b) Fit of the ground truth data of the Vaiont landslide and the calculated data by the network, (c) Fit of the ground truth data of the Shuping landslide and the calculated data by the network, (d) Fit of the ground truth data of the Mud Creek landslide and the calculated data by the network.

network that tackles the solution of the partial differential equation. Physics informed Neural Networks are promising tools for solving PDEs in multiple domains, including landslides.

In this study, we have considered three different case studies of deep-seated landslides triggered by different phenomena, and we have trained the network based on the real (field) data. Since the range of each input variable varies, data normalization has become crucial to achieve a more optimal training and forecast of the behavior of each landslide.

Moreover, in this study we have presented different network architectures, as well as different hyper-parameters. The number of layers and number of neurons play important roles in reaching an accurate solution (i.e., reproduce the real behavior of the landslide). We have also explored the best solution to minimize the mean absolute error for the three case studies and its robustness (to cater to the random process). The results presented in this paper show that a

good generalization can be achieved, which can help significantly in the development of real-time monitoring and early warning systems for catastrophic deep-seated landslides.

Declarations

- Conflict of interest: The authors declare that they have no conflict of interest.
- Availability of data and materials: The data used in this study are openly available at: https://github.com/Ahmadmoein/Landslide/raw/main/Synthetic_data.xlsx

References

(1992) Proceedings of the meeting on the 1963 Vaiont landslide, vol 1, pp 1-218, IAEG Italian Section and Dip Sci Geologiche e Paleontologiche, University of Ferrara

Abadi M, Agarwal A, Barham P, et al (2016) Tensorflow: Large-scale machine learning on heterogeneous distributed systems. arXiv preprint arXiv:160304467

Alonso E, Zervos A, Pinyol N (2016) Thermo-poro-mechanical analysis of landslides: from creeping behaviour to catastrophic failure. Géotechnique 66(3):202–219

Alonso EE, Pinyol NM (2010) Criteria for rapid sliding i. a review of vaiont case. Engineering Geology 114(3-4):198–210

Amini D, Haghighat E, Juanes R (2022) Physics-informed neural network solution of thermo-hydro-mechanical (thm) processes in porous media. arXiv

preprint arXiv:220301514

Anderson D (1980) An earthquake induced heat mechanism to explain the loss of strength of large rock and earth slides. In: Engineering for Protection from Natural Disasters, Proceedings of the International Conference, Bangkok, January 7–9, pp 569–580

Bandai T, Ghezzehei TA (2021) Physics-informed neural networks with monotonicity constraints for richardson-richards equation: Estimation of constitutive relationships and soil water flux density from volumetric water content measurements. Water Resources Research 57(2):e2020WR027,642

Baydin AG, Pearlmutter BA, Radul AA, et al (2018) Automatic differentiation in machine learning: a survey. Journal of machine learning research 18

Berg J, Nyström K (2018) A unified deep artificial neural network approach to partial differential equations in complex geometries. Neurocomputing 317:28–41

Bergstra J, Breuleux O, Bastien F, et al (2010) Theano: a cpu and gpu math expression compiler. In: Proceedings of the Python for scientific computing conference (SciPy), Austin, TX, pp 1–7

Bishop CM, Nasrabadi NM (2006) Pattern recognition and machine learning, vol 4. Springer

Brenner M, Eldredge J, Freund J (2019) Perspective on machine learning for advancing fluid mechanics. Physical Review Fluids 4(10):100,501

Brunton SL, Kutz JN (2019) Methods for data-driven multiscale model discovery for materials. Journal of Physics: Materials 2(4):044,002

Brunton SL, Noack BR, Koumoutsakos P (2020) Machine learning for fluid mechanics. Annual Review of Fluid Mechanics 52:477–508

Butler KT, Davies DW, Cartwright H, et al (2018) Machine learning for molecular and materials science. Nature 559(7715):547–555

Cai S, Wang Z, Fuest F, et al (2021a) Flow over an espresso cup: inferring 3-d velocity and pressure fields from tomographic background oriented schlieren via physics-informed neural networks. Journal of Fluid Mechanics 915

Cai S, Wang Z, Wang S, et al (2021b) Physics-informed neural networks for heat transfer problems. Journal of Heat Transfer 143(6)

Cai S, Mao Z, Wang Z, et al (2022) Physics-informed neural networks (pinns) for fluid mechanics: A review. Acta Mechanica Sinica pp 1–12

Cecinato F, Zervos A, Veveakis E, et al (2008) Numerical modelling of the thermo-mechanical behaviour of soils in catastrophic landslides. In: Landslides and Engineered Slopes. From the Past to the Future, Two Volumes+ CD-ROM. CRC Press, p 637–644

Chan TF, Keller H (1982) Arc-length continuation and multigrid techniques for nonlinear elliptic eigenvalue problems. SIAM Journal on Scientific and Statistical Computing 3(2):173–194

Chollet F, et al (2015) keras

DeVore RA (1998) Nonlinear approximation. Acta numerica 7:51–150

Ermoliev YM, Wets RB (1988) Numerical techniques for stochastic optimization. Springer-Verlag

Ferri F, Di Toro G, Hirose T, et al (2011) Low-to high-velocity frictional properties of the clay-rich gouges from the slipping zone of the 1963 vaiont slide, northern italy. Journal of Geophysical Research: Solid Earth 116(B9)

Goren L, Aharonov E (2009) On the stability of landslides: A thermo-poroelastic approach. Earth and Planetary Science Letters 277(3-4):365–372

Griewank A, et al (1989) On automatic differentiation. Mathematical Programming: recent developments and applications 6(6):83–107

Gruntfest I (1963) Thermal feedback in liquid flow; plane shear at constant stress. Transactions of the Society of Rheology 7(1):195–207

Guo M, Haghighat E (2020) An energy-based error bound of physics-informed neural network solutions in elasticity. arXiv preprint arXiv:201009088

Haghighat E, Juanes R (2021) Sciann: A keras/tensorflow wrapper for scientific computations and physics-informed deep learning using artificial neural networks. Computer Methods in Applied Mechanics and Engineering 373:113,552

Haghighat E, Raissi M, Moure A, et al (2021) A physics-informed deep learning framework for inversion and surrogate modeling in solid mechanics. Computer Methods in Applied Mechanics and Engineering 379:113,741

Handwerger AL, Huang MH, Fielding EJ, et al (2019) A shift from drought to extreme rainfall drives a stable landslide to catastrophic failure. Scientific reports 9(1):1–12

Hangelbroek T, Ron A (2010) Nonlinear approximation using gaussian kernels. Journal of Functional Analysis 259(1):203–219

Hawkins DM (2004) The problem of overfitting. Journal of chemical information and computer sciences 44(1):1–12

Huang H, Yi W, Lu S, et al (2016) Use of monitoring data to interpret active landslide movements and hydrological triggers in three gorges reservoir. Journal of Performance of Constructed Facilities 30(1):C4014,005

Hueckel T, Baldi G (1990) Thermoplasticity of saturated clays: experimental constitutive study. Journal of geotechnical engineering 116(12):1778–1796

Jagtap AD, Mitsotakis D, Karniadakis GE (2022) Deep learning of inverse water waves problems using multi-fidelity data: Application to serre–green–naghdi equations. Ocean Engineering 248:110,775

Jin X, Cai S, Li H, et al (2021) Nsfnets (navier-stokes flow nets): Physics-informed neural networks for the incompressible navier-stokes equations. Journal of Computational Physics 426:109,951

Kilburn CR, Petley DN (2003) Forecasting giant, catastrophic slope collapse: lessons from vajont, northern italy. Geomorphology 54(1-2):21–32

Kingma DP, Ba J (2014) Adam: A method for stochastic optimization. arXiv preprint arXiv:14126980

Lachenbruch AH (1980) Frictional heating, fluid pressure, and the resistance to fault motion. Journal of Geophysical Research: Solid Earth 85(B11):6097–6112

LeCun Y, Bengio Y, Hinton G (2015) Deep learning. nature 521(7553):436–444

MULLER L (1964) The rock slide of the vajont. Valley Rock Mechanics and Engineering Geology 2:3–4

Müller L (1968) New considerations on the vaiont slide. Rock Mechanics & Engineering Geology

Niaki SA, Haghighat E, Campbell T, et al (2021) Physics-informed neural network for modelling the thermochemical curing process of composite-tool systems during manufacture. Computer Methods in Applied Mechanics and Engineering 384:113,959

Pang G, Karniadakis GE (2020) Physics-informed learning machines for partial differential equations: Gaussian processes versus neural networks. In: Emerging Frontiers in Nonlinear Science. Springer, p 323–343

Paszke A, Gross S, Chintala S, et al (2017) Automatic differentiation in pytorch

Rafiei MH, Adeli H (2017) A novel machine learning-based algorithm to detect damage in high-rise building structures. The Structural Design of Tall and Special Buildings 26(18):e1400

Raissi M, Perdikaris P, Karniadakis GE (2019) Physics-informed neural networks: A deep learning framework for solving forward and inverse problems involving nonlinear partial differential equations. Journal of Computational physics 378:686–707

Rao C, Sun H, Liu Y (2021) Physics-informed deep learning for computational elastodynamics without labeled data. Journal of Engineering Mechanics 147(8):04021,043

Rice JR (2006) Heating and weakening of faults during earthquake slip. Journal of Geophysical Research: Solid Earth 111(B5)

Ruder S (2016) An overview of gradient descent optimization algorithms. arXiv preprint arXiv:160904747

Saito M (1965) Forecasting the time of occurrence of a slope failure. In: Proc. 6 th Int. Conf. Soil Mechanics and Foundation Eng., pp 537–541

Saito M (1969) Forecasting time of slope failure by tertiary creep. In: Proc. 7th Int. Conf on Soil Mechanics and Foundation Engineering, Mexico City, Citeseer, pp 677–683

Schmidhuber J (2015) Deep learning in neural networks: An overview. Neural networks 61:85–117

Seguí C (2020) Analysis of the Stability and Response of Deep-Seated Landslides by Monitoring their Basal Temperature. PhD thesis, Duke University, URL https://hdl.handle.net/10161/22193

Seguí C, Veveakis M (2022) Fusing physics-based and data-driven models to forecast and mitigate landslide collapse. California Digital Library (CDL) https://doi.org/https://doi.org/10.31223/X5W642

Segui C, Rattez H, Veveakis M (2020) On the stability of deep-seated landslides. the cases of vaiont (italy) and shuping (three gorges dam, china). Journal of Geophysical Research: Earth Surface 125(7):e2019JF005,203

Seguí C, Tauler E, Planas X, et al (2021) The interplay between phyllosilicates fabric and mechanical response of deep-seated landslides. the case of el forn de canillo landslide (andorra). Landslides 18(1):145–160

Sibi P, Jones SA, Siddarth P (2013) Analysis of different activation functions using back propagation neural networks. Journal of theoretical and applied

information technology 47(3):1264–1268

Tariyal S, Majumdar A, Singh R, et al (2016) Greedy deep dictionary learning. arXiv preprint arXiv:160200203

Vardoulakis I (2002a) Dynamic thermo-poro-mechanical analysis of catastrophic landslides. Geotechnique 52(3):157–171

Vardoulakis I (2002b) Steady shear and thermal run-away in clayey gouges. International journal of solids and structures 39(13-14):3831–3844

Veveakis E, Vardoulakis I, Di Toro G (2007) Thermoporomechanics of creeping landslides: The 1963 vaiont slide, northern italy. Journal of Geophysical Research: Earth Surface 112(F3)

Veveakis E, Alevizos S, Vardoulakis I (2010) Chemical reaction capping of thermal instabilities during shear of frictional faults. Journal of the Mechanics and Physics of Solids 58(9):1175–1194

Voight B (1988) A method for prediction of volcanic eruptions. Nature 332(6160):125–130

Voight B, Faust C (1982) Frictional heat and strength loss in some rapid landslides. Geotechnique 32(1):43–54

Wang DJ, Tang HM, Zhang YH, et al (2017) An improved approach for evaluating the time-dependent stability of colluvial landslides during intense rainfall. Environmental Earth Sciences 76(8):1–12

Wu JL, Xiao H, Paterson E (2018) Physics-informed machine learning approach for augmenting turbulence models: A comprehensive framework. Physical Review Fluids 3(7):074,602

Yoon CE, O'Reilly O, Bergen KJ, et al (2015) Earthquake detection through computationally efficient similarity search. Science advances 1(11):e1501,057